galaxies

MDPI

Article

Magnetic Noise Mitigation Strategies for the Einstein Telescope Infrastructure

Barbara Garaventa [1,*], Federico Armato [1], Andrea Chincarini [1] and Irene Fiori [2]

[1] INFN Genova, 16146 Genova, Italy; federico.armato@ge.infn.it (F.A.); andrea.chincarini@ge.infn.it (A.C.)
[2] European Gravitational Observatory, 56021 Cascina, Italy; irene.fiori@ego-gw.it
* Correspondence: barbara.garaventa@ge.infn.it

Abstract: The Einstein Telescope (ET) will be a third-generation Gravitational Wave (GW) detector that will tackle cutting-edge technological challenges. The ET will be constructed at a depth of 200–300 m to isolate it from vibrations caused by seismic waves and human activities, which are sources of noise for GW detection. To meet the ET's objectives, it will be necessary to improve low-frequency sensitivity by about two orders of magnitude compared to current interferometers (LIGO, Virgo). Magnetic noise is a limiting noise in the frequency range from a few Hz up to around 100 Hz in future GW detectors. This article will discuss the magnetic noise mitigation strategies under development, based on experiences from Virgo.

Keywords: gravitational waves; magnetic noise; Einstein Telescope

1. Introduction

Current gravitational wave detectors employ cutting-edge techniques to capture the "sounds" of the universe—gravitational waves—using laser interferometry. The sensitivity of these interferometers is constrained by various sources of noise, and the primary objective is to mitigate these sources to optimize sensitivity, enabling us to explore the universe with greater depth.

The Einstein Telescope is a future third-generation gravitational wave detector that will be built underground, at a depth of approximately 200 m, to reduce specific noise sources present in current interferometers, such as seismic noise and anthropogenic noise [1]. This will optimize the detector's sensitivity in the medium-to-low-frequency range, which is particularly relevant for signals between 1 and 100 Hz, while also complementing the broader frequency range of current detectors, which extends from about 10 Hz to several kHz.

The Einstein Telescope will also need to equip its infrastructure to mitigate magnetic noise, which is a source of noise that limits the frequency range from a few Hz up to around 100 Hz [2]. Magnetic noise primarily arises from two sources: the natural terrestrial component and the environmental noise component of the interferometer. The first is due to Schumann resonances [3], typically of the order of $pT/\sqrt{Hz}$, which are caused by electromagnetic signals excited in the cavity formed between the Earth's surface and the ionosphere [4,5]. The second is the so-called "self-inflicted" noise, generated by devices carrying electric current, such as power grid cables, motors, and pumps.

To reduce environmental magnetic noise, the first step is to identify the devices and wirings that contribute the most. Once these critical elements are identified, they should, whenever possible, be positioned away from the interferometer's sensitive components.

check for updates

Academic Editor: Eleonora Troja

Received: 15 December 2024
Revised: 24 January 2025
Accepted: 26 January 2025
Published: 31 January 2025

Citation: Garaventa, B.; Armato, F.; Chincarini, A.; Fiori, I. Magnetic Noise Mitigation Strategies for the Einstein Telescope Infrastructure. *Galaxies* **2025**, *13*, 9. https://doi.org/10.3390/galaxies13010009

Additionally, their magnetic emissions should be minimized through effective geometric configurations (such as cable twisting) or by applying shielding techniques, as outlined in this paper.

The presence of magnetic noise in interferometers such as Virgo [6] and LIGO [7] is caused by the coupling of environmental magnetic fields—originating from devices like Faraday isolators mounted on suspended optical benches—with magnetized components of the detector. This coupling can induce both direct magnetic forces and disturbances in the control signals, contributing to noise in the detector's sensitivity range [8].

A significant magnetic coupling in the Virgo interferometer occurs with the permanent magnets of the mirrors, which are the primary sensitive components of the interferometer (Figure 1).

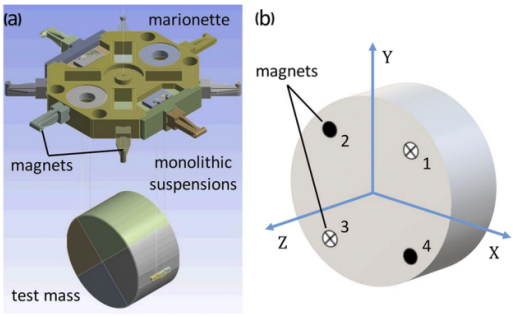

Figure 1. (**a**) Schematics of the last suspension stage of the Virgo TM, which includes the marionette with 8 actuation magnets, 4 fused silica suspension fibres, and the TM itself; (**b**) schematic view of the cross anti-parallel configuration of the 4 magnets glued on the Virgo TM [9].

For the Einstein Telescope, it will be necessary to mitigate these sources of magnetic noise, building on the experience gained from current gravitational wave interferometers, such as Virgo and KAGRA [10]. To achieve the targets for the ET, it will be essential to reduce environmental magnetic fields to the level of terrestrial noise and decrease magnetic couplings by a factor of approximately 10^2–10^3 compared to current GW detectors [2].

2. Magnetic Noise Investigation

Building on the experience gained with the Virgo (Italy) and KAGRA (Japan) interferometers, it is possible to outline general guidelines for minimizing ambient magnetic couplings. Specifically, Virgo is more affected by "self-inflicted" noise compared to the quieter magnetic environment of KAGRA. Particular attention must be paid to the management of power distribution systems near the interferometer's sensitive zones, such as the test masses. This includes mitigating electromagnetic fields radiated by cables and wires, as well as magnetic fields from electrical and electronic devices.

A method currently used in Virgo to estimate magnetic couplings, known as Coupling Functions (CFs), involves magnetic injections at various coupling points, specifically the interferometer towers [11]. These injections are carried out using a far-field approach (with a large coil, BC in Equation (1)) and a near-field approach (with a small coil, SC in Equation (1)). The CFs of individual towers, weighted by coefficients (alpha), are combined with the magnetic field intensity measured by the magnetometers at each tower during the far-field injection. This approach allows for a precise characterization of the magnetic coupling at different points within the system:

$$CF_{BC}(f) = \sum_{i}^{N} \alpha_i CF_{i,SC}(f), \quad (1)$$

where N is the number of the towers and α_i is estimated by the fitting of measured CF_{BC} with a linear combination of $CF_{i,SC}$. Another crucial aspect of investigating magnetic noise involves environmental factors, such as acoustic, seismic, and magnetic noise sources, including railways [12]. For instance, in Virgo, it has been shown that there is a correlated magnetic pattern associated with trains as they change speed while approaching a station. This aspect will be crucial when assessing potential excess magnetic noise, as the Einstein Telescope is much more sensitive to low frequencies compared to currently operational interferometers.

MANET Facility

MANET (MAgnetic Noise test facility for ET) is a specialized test bench designed to advance the development of the Einstein Telescope (ET). Its primary objectives are to characterize the magnetic noise emissions of various devices, analyze their response to external magnetic fields, and evaluate magnetic mitigation strategies.

At the core of MANET is a rotating table, where devices under study are positioned (Figure 2). Surrounding this table is an array of magnetic sensors strategically positioned to measure the magnetic field at various angles (Figure 3).

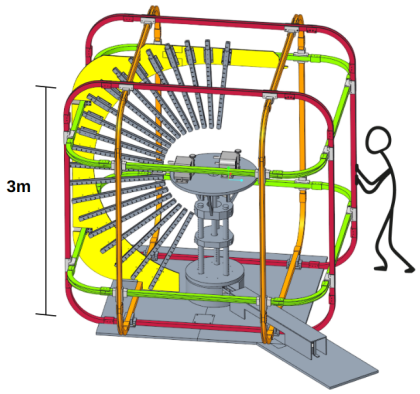

Figure 2. MANET facility design. The structure is almost entirely made of plastic and non-magnetic stainless steel to avoid altering the system being characterized.

This setup enables the precise characterization of the device's magnetic properties, including its magnetic moment and the lower-order terms of its multipole expansion.

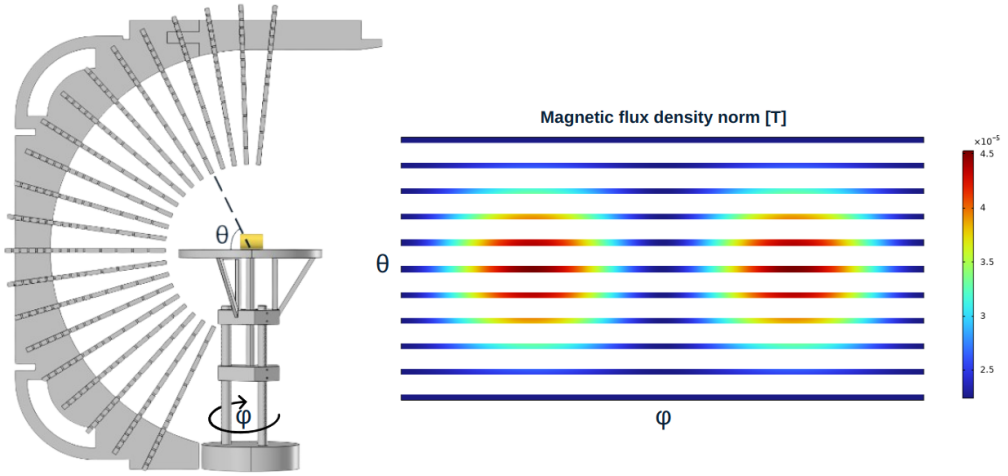

Figure 3. Simulation with COMSOL Multiphysics software of the magnetic field of an ideal dipole as it will be observed by MANET.

MANET is further equipped with a system of three pairs of Helmholtz coils, which generate uniform magnetic fields in controlled directions. This feature allows for the detailed testing of a device's response to external fields and the evaluation of different mitigation techniques to reduce magnetic interference.

The facility is set to become operational early next year and will play a crucial role in advancing the development of the ET.

3. Magnetic Noise Mitigation

To minimize magnetic couplings, it is essential to shield the most sensitive areas in GW interferometers.

An important parameter is the Shielding Factor (SF), which is the ratio between the magnetic field before and after applying shielding techniques.

In order to mitigate magnetic noise, both active and passive techniques can be employed. The former includes Helmholtz coils. The latter includes eddy currents, where a changing flux, as described by Faraday's law, generates an induced magnetic field that partially cancels the one from the source; ferromagnetic shields, which can attract and move magnetic field lines away from the area where it is necessary to mitigate.

In the following sub-sections, simulations on mitigation strategies, using COMSOL Multiphysics software, will be applied to the Test Mass (TM) tower, one of the most sensitive components, using Virgo as reference.

3.1. Ferromagnetic Shielding

A proposed shielding of the TM tower involves covering the tower and the interferometer arms near the intersection area with a layer of material with high magnetic permeability. Specifically, the simulations varied the thickness of the layer, its relative magnetic permeability, and the extent of the covered area.

The magnetic field in the intersection region decreases with an increasing thickness of the layer (Table 1) and its relative magnetic permeability (Table 2). The following tables show two different cases of a static uniform external magnetic field direction: a field along the axis of one arm and a field at 45° with respect to the interferometer arms.

Table 1. Shielding factor achieved in the center of the intersection area by covering the interferometer arms with a ferromagnetic layer with a relative magnetic permeability of 100,000 over a length of 2 m.

Thickness (mm)	Shielding Factor ($\mathbf{B}_{ext} = B\hat{x}$)	Shielding Factor ($\mathbf{B}_{ext} = \frac{B}{\sqrt{2}}(\hat{x}, \hat{y})$)
0.4	3.92	3.62
0.8	4.81	4.42
1.2	5.66	5.19
1.6	6.48	5.95
2.0	7.29	6.68

However, as shown in Figures 4 and 5, increasing the coverage area of the arms with high-permeability material beyond a certain size—determined by the geometry—does not further reduce the magnetic field in the intersection region. Instead, it simply extends the area where the field is mitigated.

Such shielding can be constructed using mu-metal sheets, a ferromagnetic material known for its exceptionally high relative magnetic permeability, which can reach values of up to approximately 100,000 under optimal conditions. However, early attempts to utilize this material indicate that bending or mechanical stress on the sheets can degrade their magnetic properties, leading to a noticeable reduction in their relative magnetic permeability.

Table 2. Shielding factor achieved in the center of the intersection area by covering the interferometer arms with a 2 mm-thick layer over a length of 2 m.

μ_r	Shielding Factor ($B_{ext} = B\hat{x}$)	Shielding Factor ($B_{ext} = \frac{B}{\sqrt{2}}(\hat{x}, \hat{y})$)
1000	3.01	2.80
2000	3.05	2.85
5000	3.20	2.98
10,000	3.45	3.19
20,000	3.92	3.62
50,000	5.23	4.81
100,000	7.29	6.68

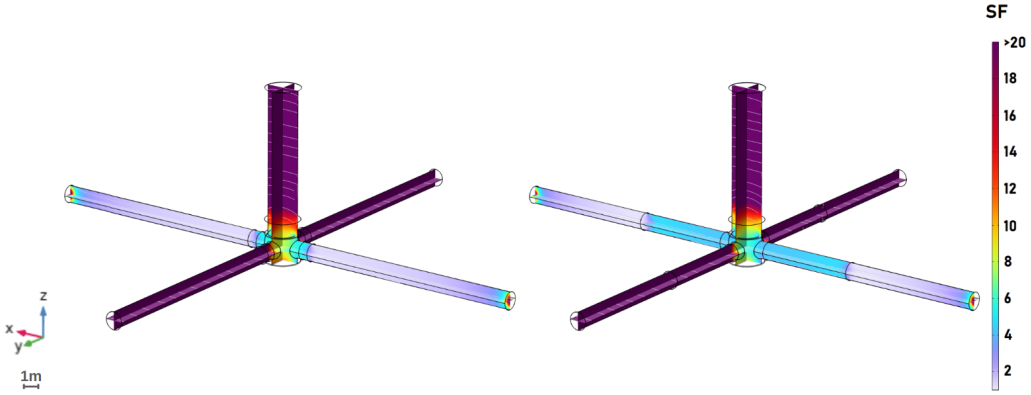

Figure 4. Shielding factor achieved by covering the interferometer arms with a 2 mm-thick layer of a ferromagnetic layer with a relative magnetic permeability of 100,000 over lengths of 1 m (**left** figure) and 5 m (**right** figure), respectively. The external uniform magnetic field is directed along one arm of the interferometer.

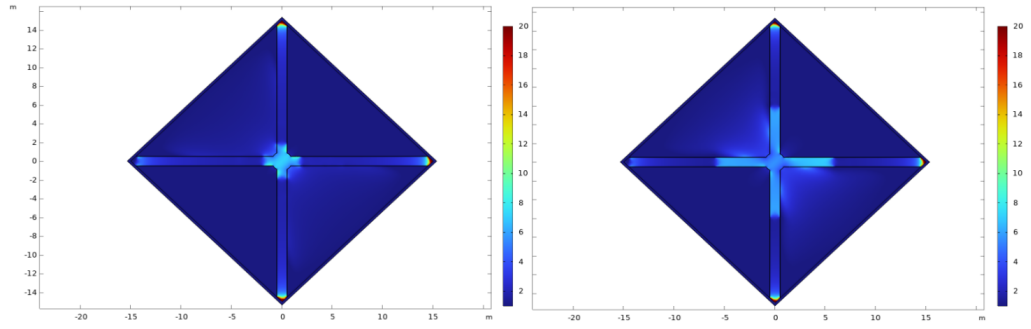

Figure 5. Shielding factor achieved by covering the interferometer arms with a 2 mm-thick layer of a ferromagnetic layer with a relative magnetic permeability of 100,000 over lengths of 1 m (**left** figure) and 5 m (**right** figure), respectively. The external uniform magnetic field is at 45° with respect to the interferometer arms.

3.2. Eddy Currents

Another proposed shielding method for the TM tower involves exploiting eddy currents by enclosing the interferometer arms at their intersection with hollow cylinders made of conductive material.

In the simulations, the two pairs of cylinders are arranged in a Helmholtz configuration, where the cylinders in each pair are separated by a distance equal to their respective radius (Figure 6). The radius is 2.05 m for the pair aligned along the x-axis and 2 m for the pair aligned along the y-axis. The radii of the two pairs must differ to avoid overlap between the cylinders.

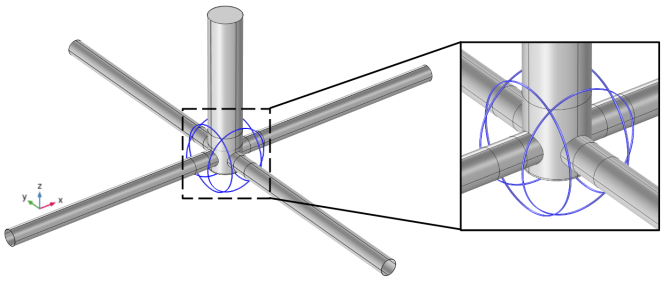

Figure 6. In blue, the two pairs of cylinders are arranged in a Helmholtz configuration. The radius is 2.05 m for the pair aligned along the x-axis and 2 m for the pair aligned along the y-axis.

Table 3 presents the shielding factor as a function of the external field frequency, with the thickness of the hollow cylinders set to 2 cm and their height to 5 cm. Tables 4 and 5 show how the shielding factor varies with the thickness and height of the cylinders, respectively.

Table 3. Shielding factor achieved at the center of the intersection area. The cylinders have a thickness of 2 cm and a height of 5 cm. The shielding factor is provided as a function of both the frequency and the direction of the external field.

Frequency Hz	SF ($B_{ext} = B\hat{x}$)	SF ($B_{ext} = \frac{B}{\sqrt{2}}(\hat{x}, \hat{y})$)	SF ($B_{ext} = B\hat{y}$)
1000	1.836	1.845	1.836
2000	1.837	1.847	1.837
5000	1.838	1.848	1.838
10,000	1.838	1.848	1.838

Table 4. Shielding factor achieved at the center of the intersection area. The cylinders have a height of 5 cm. The external field is set to a frequency of 1000 Hz. The shielding factor is provided as a function of both the direction of the external field and the thickness of the cylinders.

Thickness (cm)	SF ($B_{ext} = B\hat{x}$)	SF ($B_{ext} = \frac{B}{\sqrt{2}}(\hat{x}, \hat{y})$)	SF ($B_{ext} = B\hat{y}$)
0.4	1.773	1.772	1.773
0.8	1.781	1.783	1.790
1.2	1.804	1.806	1.809
1.6	1.823	1.825	1.825
2.0	1.836	1.845	1.836

Table 5. Shielding factor achieved at the center of the intersection area. The cylinders have a thickness of 2 cm. The external field is set to a frequency of 1000 Hz. The shielding factor is provided as a function of both the direction of the external field and the height of the cylinders.

Height (cm)	SF ($B_{ext} = B\hat{x}$)	SF ($B_{ext} = \frac{B}{\sqrt{2}}(\hat{x}, \hat{y})$)	SF ($B_{ext} = B\hat{y}$)
5	1.836	1.845	1.836
10	2.061	2.058	2.055

In a second configuration, the pairs of cylinders, still arranged in a Helmholtz configuration, are placed inside the tower (Figure 7). In this case, the radius of the pair aligned along the x-axis is 0.55 m while the radius of the pair aligned along the y-axis is 0.5 m.

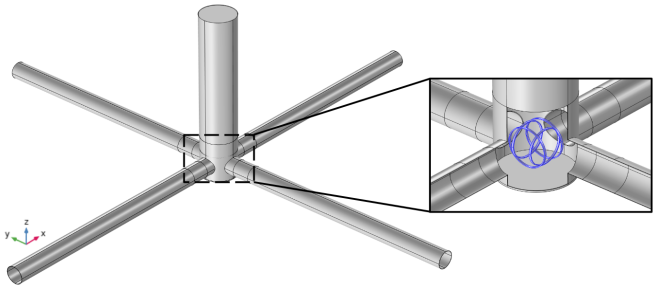

Figure 7. In blue, the two pairs of cylinders are arranged in a Helmholtz configuration. The radius is 0.55 m for the pair aligned along the x-axis and 0.5 m for the pair aligned along the y-axis.

Table 6 presents the shielding factor as a function of the external field frequency, with the thickness of the hollow cylinders set to 2 cm and their height set to 5 cm. Tables 7 and 8 keep the frequency fixed at 500 Hz, highlighting how the shielding factor varies with the thickness and height of the cylinders, respectively.

Table 6. Shielding factor achieved at the center of the intersection area. The cylinders have a thickness of 2 cm and a height of 5 cm. The shielding factor is provided as a function of both the frequency and the direction of the external field.

Frequency Hz	SF ($\mathbf{B}_{ext} = B\hat{x}$)	SF ($\mathbf{B}_{ext} = \frac{B}{\sqrt{2}}(\hat{x}, \hat{y})$)	SF ($\mathbf{B}_{ext} = B\hat{y}$)
100	2.338	2.394	2.436
200	2.397	2.457	2.502
500	2.435	2.498	2.546
1000	2.449	2.513	2.562
2000	2.455	2.519	2.569
5000	2.457	2.521	2.571
10,000	2.458	2.522	2.572

Table 7. Shielding factor achieved at the center of the intersection area. The cylinders have a height of 5 cm. The external field is set to a frequency of 500 Hz. The shielding factor is provided as a function of both the direction of the external field and the thickness of the cylinders.

Thickness (cm)	SF ($\mathbf{B}_{ext} = B\hat{x}$)	SF ($\mathbf{B}_{ext} = \frac{B}{\sqrt{2}}(\hat{x}, \hat{y})$)	SF ($\mathbf{B}_{ext} = B\hat{y}$)
0.4	2.240	2.260	2.275
0.8	2.308	2.329	2.355
1.2	2.356	2.369	2.401
1.6	2.417	2.444	2.472
2.0	2.435	2.498	2.546

Table 8. Shielding factor achieved at the center of the intersection area. The cylinders have a thickness of 2 cm. The external field is set to a frequency of 500 Hz. The shielding factor is provided as a function of both the direction of the external field and the height of the cylinders.

Height (cm)	SF ($\mathbf{B}_{ext} = B\hat{x}$)	SF ($\mathbf{B}_{ext} = \frac{B}{\sqrt{2}}(\hat{x}, \hat{y})$)	SF ($\mathbf{B}_{ext} = B\hat{y}$)
5	2.435	2.498	2.546
10	2.916	3.109	3.096

As shown in the tables, changing the characteristics of the hollow cylinder (such as thickness and height) and varying the frequencies of the external magnetic field do not lead to a significant improvement in the shielding factor. While an increase in frequency is expected to enhance the shielding factor due to stronger induced currents, the results

suggest—consistent with the theory—that the induced currents primarily work to minimize the magnetic field within the cylinder itself, rather than reducing the field between the two cylinders. Indeed, the second configuration, where the cylinders are placed inside the towers, yields better results because the area to be shielded is geometrically closer to the surface covered by the cylinder.

4. Discussion

This article introduces two passive magnetic noise mitigation strategies applied to the TM tower. The first strategy, implemented at the simulation level, involves introducing a layer of high-magnetic-permeability material (e.g., mu-metal) to redirect magnetic field lines. The second strategy leverages eddy currents by enclosing the interferometer arms and the tower at the intersection regions with hollow cylinders made of conductive material (e.g., aluminum). In the simulations, the cylinders are considered ideal, meaning that potential nonlinearities—such as those arising from material processing—are not accounted for, which could influence the shielding factor.

Future developments of these simulations will investigate the advantages of multi-layer systems, including active ones, and evaluate the use of both hollow aluminum cylinders and ferromagnetic shielding. Moreover, the implementation of these shielding techniques will be explored to minimize "self-inflicted" magnetic noise by directly shielding the noise sources themselves (e.g., the Faraday isolators).

Simulations in the low-frequency range (1–100 Hz) were not carried out due to the constraints of the software employed. A next step will be to perform a fit to estimate the effectiveness of Helmholtz Coils at low frequencies.

Furthermore, the article introduces MANET, a new facility developed by the INFN group in Genoa. This facility will enable the characterization of devices' magnetic emissions, facilitating the development of effective mitigation strategies. Additionally, it will allow for the validation of these strategies and the characterization of shielding materials both before and after processing, ensuring the accurate determination of shielding factor values.

5. Conclusions

This paper presents strategies for mitigating magnetic noise, which will be essential for future gravitational wave detectors, such as the Einstein Telescope. Drawing from the experiences of current GW detectors, Virgo and KAGRA, a set of guidelines has been developed to reduce the magnetic coupling with the test masses of the interferometer. Furthermore, this article introduces a new instrument, MANET, which will be installed next year at the EGO-Virgo site. MANET will serve as a test bench for the Einstein Telescope, providing valuable insights and tools for further advancements in magnetic noise mitigation.

Author Contributions: Conceptualization, A.C.; methodology, F.A., A.C. and B.G.; formal analysis, F.A. and B.G.; investigation, F.A. and B.G.; data curation, F.A. and B.G; writing—original draft preparation, F.A. and B.G.; writing—review and editing, F.A. and B.G.; supervision, F.A., A.C., I.F. and B.G.; funding acquisition, A.C. All authors have read and agreed to the published version of the manuscript.

Funding: This research received external funding from PNRR ETIC-Einstein Telescope Infrastructure Consortium IR0000004–CUP I53C21000420006.

Data Availability Statement: Data supporting the reported results are unavailable. The materials were imported from the libraries of COMSOL Multiphysics software.

Acknowledgments: Thanks to EGO-Virgo team and INFN technicians support for their collaboration.

Conflicts of Interest: The authors declare no conflicts of interest.

Abbreviations

The following abbreviations are used in this manuscript:

CF	Coupling Function
ET	Einstein Telescope
GWs	Gravitational Waves
KAGRA	Kamioka Gravitational Wave Detector
LIGO	Laser Interferometer Gravitational-wave Observatory
MANET	MAgnetic Noise test facility for ET
SF	Shielding Factor
TM	Test Mass

References

1. Punturo, M.; Abernathy, M.; Acernese, F.; Allen, B.; Andersson, N.; Arun, K.; Barone, F.; Barr, B.; Barsuglia, M.; Beker, M.; et al. The Einstein Telescope: A third-generation gravitational wave observatory. *Class. Quantum Grav.* **2010**, *27*, 194002. [CrossRef]
2. Amann, F.; Bonsignorio, F.; Bulik, T.; Bulten, H.J.; Cuccuru, S.; Dassargues, A.; DeSalvo, R.; Fenyvesi, E.; Fidecaro, F.; Fiori, I.; et al. Site-selection criteria for the Einstein Telescope. *Rev. Sci. Instrum.* **2020**, *91*, 094504. [CrossRef] [PubMed]
3. Schumann, W.O. Über die strahlungslosen Eigenschwingungen einer leitenden Kugel, die von einer Luftschicht und einer Ionosphärenhülle umgeben ist. *Zeitschrift Naturforschung A* **1952**, *7*, 149–154. [CrossRef]
4. Schumann, W.O. Über die Dämpfung der elektromagnetischen Eigenschwingungen des Systems Erde-Luft-Ionosphäre. *Zeitschrift Naturforschung A* **1952**, *7*, 250–252. [CrossRef]
5. Janssens, K.; Martinovic, K.; Christensen, N.; Meyers, P.M.; Sakellariadou, M. Impact of Schumann resonances on the Einstein Telescope and projections for the magnetic coupling function. *Phys. Rev. D* **2021**, *104*, 122006, Erratum in *Phys. Rev. D* **2022**, *105*, 109904. [CrossRef]
6. Acernese, F.; Adams, T.; Agatsuma, K.; Aiello, L.; Allocca, A.; Amato, A.; Antier, S.; Arnaud, N.; Ascenzi, S.T.; Astone, P.; et al. Advanced Virgo Status. *J. Phys. Conf. Ser.* **2020**, *1342*, 012010. [CrossRef]
7. Aasi, J.; Abbott, B.P.; Abbott, R.; Abbott, T.; Abernathy, M.R.; Ackley, K.; Adams, C.; Adams, T.; Addesso, P.; Adhikari, R.X.; et al. Advanced LIGO. *Class. Quantum Grav.* **2015**, *32*, 074001.
8. Cirone, A.; Fiori, I.; Paoletti, F.; Perez, M.M.; Rodríguez, A.R.; Swinkels, B.L.; Vazquez, A.M.; Gemme, G.; Chincarini, A. Investigation of magnetic noise in advanced Virgo. *Class. Quantum Gravity* **2019**, *36*, 225004. [CrossRef]
9. Cirone, A.; Chincarini, A.; Neri, M.; Farinon, S.; Gemme, G.; Fiori, I.; Paoletti, F.; Majorana, E.; Puppo, P.; Rapagnani, P.; et al. Magnetic coupling to the advanced Virgo payloads and its impact on the low frequency sensitivity. *Rev. Sci. Instrum.* **2018**, *89*, 114501. [CrossRef] [PubMed]
10. Akutsu, T.; Ando, M.; Arai, K.; Arai, Y.; Araki, S.; Araya, A.; Aritomi, N.; Asada, H.; Aso, Y.; Atsuta, S.; et al. KAGRA: 2.5 Generation Interferometric Gravitational Wave Detector. *Nat. Astron.* **2019**, *3*, 35–40.
11. Fiori, I.; Paoletti, F.; Tringali, M.C.; Janssens, K.; Karathanasis, C.; Menéndez-Vázquez, A.; Romero-Rodríguez, A.; Sugimoto, R.; Washimi, T.; Boschi, V.; et al. The Hunt for Environmental Noise in Virgo during the Third Observing Run *Galaxies* **2020**, *8*, 82. [CrossRef]
12. Lowes, F.J. DC railways and the magnetic fields they produce—The geomagnetic context. *Earth Planet Space* **2009**, *61*, i–xv. [CrossRef]